Density probability distribution in one-dimensional polytropic gas dynamics

Thierry Passot
Observatoire de la Côte d'Azur, Boîte Postale 4229, 06304, Nice Cedex 4, France

Enrique Vázquez-Semadeni
Instituto de Astronomía, UNAM, Apartado Postal 70-264, México, Distrito Federal 04510, Mexico

(Received 5 February 1998)

We discuss the generation and statistics of the density fluctuations in highly compressible polytropic turbulence, based on a simple model and one-dimensional numerical simulations. Observing that density structures tend to form in a hierarchical manner, we assume that density fluctuations follow a random multiplicative process. When the polytropic exponent γ is equal to unity, the local Mach number is independent of the density, and our assumption leads us to expect that the probability density function (PDF) of the density field is a log-normal. This isothermal case is found to be special, with a dispersion σ_s^2 scaling as the square turbulent Mach number $\tilde{M}^2$, where $s \equiv \ln \rho$ and ρ is the fluid density. Density fluctuations are stronger than expected on the sole basis of shock jumps. Extrapolating the model to the case $\gamma \neq 1$, we find that as the Mach number becomes large, the density PDF is expected to asymptotically approach a power-law regime at high densities when $\gamma < 1$, and at low densities when $\gamma > 1$. This effect can be traced back to the fact that the pressure term in the momentum equation varies exponentially with s, thus opposing the growth of fluctuations on one side of the PDF, while being negligible on the other side. This also causes the dispersion σ_s^2 to grow more slowly than $\tilde{M}^2$ when $\gamma \neq 1$. In view of these results, we suggest that Burgers flow is a singular case not approached by the high-$\tilde{M}$ limit, with a PDF that develops power laws on both sides. [S1063-651X(98)16909-X]

PACS number(s): 47.27.Ak, 47.40.Ki, 95.30.Lz

I. INTRODUCTION

The formation of density structures by the velocity field of highly compressible turbulence is of great interest in astrophysics. The determination of their typical amplitude, size and volume filling factor poses significant difficulties since it requires a knowledge of the full statistics. In this paper we shall concentrate on one-point statistics and more specifically on the probability density function (PDF) of the density fluctuations in one-dimensional (1D) turbulent flows.

It is well known that the density jump in a shock depends directly on the cooling ability of the fluid. Thus, for an adiabatic flow the maximum density jump is 4, for an isothermal flow it is $\sim M_a^2$ [1], and for nearly isobaric flows it is $\sim e^{M_a^2}$ [2], where M_a is the Mach number ahead of the shock. The net cooling ability of a flow can be conveniently parametrized by the polytropic exponent γ, so that the thermal pressure P is given by $P = K\rho^\gamma$, where ρ is the fluid density [3]. Isothermal flows have $\gamma = 1$, and isobaric flows have $\gamma = 0$. Note that $\gamma < 0$ corresponds to the isobaric mode of the thermal instability (see, e.g., [4]). Thus, in general, the amplitude of the turbulent density fluctuations will be a function of γ.

Previous work with isothermal flows had suggested that the PDF is log-normal [5,6], while for Burgers flows a power-law PDF has been reported [7]. More recently, evidence that flows with effective polytropic indices $0 < \gamma < 1$ also develop power-law tails at high densities has been presented [8]. In order to resolve this discrepancy, we present a series of 1D numerical simulations of polytropic gas turbulence with random forcing, in which the polytropic exponent γ parametrizes the compressibility of the flow. We have chosen to use 1D simulations in order to perform a large number of experiments at a sufficiently high resolution, integrated over very long time intervals, allowing us to collect large statistical samples.

The simulations have three governing parameters: the polytropic index γ, the Mach number M, and the Reynolds number R. We keep the Reynolds number fixed and explore the effects of varying γ and M on the resulting density PDF. Variation of γ induces a clear qualitative variation of the density PDF, which at large Mach number displays a power-law tail at high densities for $0 < \gamma < 1$, becomes log-normal for $\gamma = 1$, and develops a power-law tail at low densities for $\gamma > 1$. This suggests a symmetry about the case $\gamma = 1$ that we also explore. Variation of the Mach number, on the other hand, only appears to induce a quantitative change, the width of the PDF increasing with M.

The plan of the paper is as follows. In Sec. II we describe the equations solved and the numerical method. In Sec. III we describe the statistics of the various fields, in terms of their PDFs, together with a tentative model and a discussion of the Burgers case. Section IV is devoted to a discussion on the choice of the forcing, together with a summary of our results.

II. EQUATIONS AND NUMERICAL METHOD

We choose to concentrate on one-dimensional forced polytropic gas dynamics, governed by the following nondimensionalized equations:

$$\partial_t u + u\,\partial_x u = -\frac{1}{\gamma M^2}\frac{\partial_x \rho^\gamma}{\rho} + \frac{1}{R}\partial_{xx} u + a, \qquad (1)$$

$$\partial_t \rho + \partial_x(\rho u) = 0, \tag{2}$$

where u is the velocity of the fluid in units of U, ρ the density in units of ρ_0, γ the polytropic index, and M the Mach number of the unit velocity U at the unit density ρ_0. The equations are driven by an acceleration a with zero mean. The Reynolds number is $R = UL/\nu$, where L is the size of the domain and ν the kinematic viscosity chosen constant to ensure the conservation of the mean velocity $\langle u \rangle = 1/L \int u\, dx$. The viscous term is kept as small as possible and is only included to prevent numerical blowup. Note that the ''correct'' form of the viscous term is obtained after replacing ν with the ratio μ/ρ, where the dynamical viscosity μ is usually considered independent of the density. The equations then conserve the momentum $\int \rho u\, dx$ if the acceleration a in Eq. (1) is also replaced by the ratio of a force f to the density ρ. The dynamics that results in this case is very different due to the dependence of the driving term with respect to the density, as discussed in the last section.

For large Mach number simulations, it was found necessary to smooth density gradients using a mass diffusion term of the form $\mu_r \partial_{xx} \rho$ in the right-hand side of Eq. (2). Total mass is still conserved in the presence of this term, and if μ_r is taken sufficiently small, it has been tested that mass diffusion does not affect the dynamics in a way that could modify our conclusions.

It was also convenient to solve Eqs. (1) and (2) using the variable $s \equiv \ln \rho$. The numerical code uses a standard pseudospectral method with periodic boundary conditions. Time advance is performed using a Crank-Nicholson scheme for the linear terms and an Adams-Bashforth scheme for the nonlinear ones. For all the runs presented in this paper, the kinematic viscosity has been fixed at $\nu = 3 \times 10^{-3}$. For runs with $M \geqslant 3$, we have $\mu_r = 5 \times 10^{-4}$.

The acceleration a is prescribed in Fourier space. Its spectrum has a constant amplitude (equal to 0.6) on wave numbers $1 \leqslant k \leqslant 19$ and phases chosen randomly with a correlation time $t_{\mathrm{cor}} = 0.003$. Resolution ranges from $N = 3072$ to $N = 6144$ grid points for the runs with $M \geqslant 6$.

We perform one-point statistics of the simulations, for both the density and the velocity derivatives, keeping the forcing and the viscosity constant. All simulations start with zero initial velocity and constant density.

In order to obtain reasonably sampled histograms of the one-dimensional fields, which contain only N spatial data points, we sum the histograms over time, sampling at intervals of 0.1 time units, integrating over a total of 150 time units. However, we have found that, since the simulations start with uniform density, the first several samples must be discarded, since they bias the density histogram near $\rho = 1$. We typically skip the first 20 temporal samples (two time units). The PDFs thus computed contain roughly four million data points. Note that longer integration times are needed at a larger Mach number in order to reach a statistically relevant sample, the sound crossing time of the integration domain being larger as M increases.

III. A MODEL FOR THE DENSITY PDF

A. Properties of the governing equations

Before describing our model for the density PDF, it is instructive to rewrite the governing equations in the inviscid, unforced case, using the variable $v = (1-\gamma) \ln \rho$ when $\gamma \neq 1$ and $s = \ln \rho$ when $\gamma = 1$. For $\gamma \neq 1$, we get

$$\frac{Du}{Dt} = \frac{1}{(1-\gamma)M^2} \frac{\partial}{\partial x} e^{-v}, \tag{3}$$

$$\frac{Dv}{Dt} = -(1-\gamma) \frac{\partial}{\partial x} u, \tag{4}$$

and for $\gamma = 1$,

$$\frac{Du}{Dt} = -\frac{1}{M^2} \frac{\partial}{\partial x} s, \tag{5}$$

$$\frac{Ds}{Dt} = -\frac{\partial}{\partial x} u, \tag{6}$$

where D/Dt stands for the convective derivative. The variable v is, up to an additive constant, the logarithm of the square of the sound speed, and when $\gamma = 1$, it becomes identically zero.

These equations can be rewritten in Riemann invariant form. For $\gamma \neq 1$, they read

$$[\partial_t + (u \pm c)\partial_x] \left(u \pm \frac{2c}{(\gamma - 1)} \right) = 0, \tag{7}$$

where $c = \rho^{(\gamma-1)/2}/M$ is the sound speed, while in the singular case $\gamma = 1$ these equations become

$$\left[\partial_t + \left(u \pm \frac{1}{M} \right) \partial_x \right] \left(u \pm \frac{\ln \rho}{M} \right) = 0. \tag{8}$$

A number of interesting remarks can be made regarding the preceding equations.

(i) When $\gamma = 1$, Eqs. (5) and (6) are invariant upon the change $s \to s + b$, where b is an arbitrary constant. Indeed, the sound speed does not depend on the local density of the fluid in this case.

(ii) In the general case, if we replace γ with $2 - \gamma$ and ρ with $1/\rho$, we observe that the Riemann invariants $z^{\pm} = u \pm [2c/(\gamma - 1)]$ are exchanged, while their speeds $u \pm c$ remain unchanged. We shall now explore the implications of this remark on the statistics of the density fluctuations in the weakly compressible regime. For small values of the Mach number, a reductive perturbation expansion can be performed on the viscous equations and it has been shown [9] (see also [10]) that one-dimensional compressible turbulence reduces essentially to the superposition of the solutions of two Burgers equations describing nonlinear wave propagation in opposite directions. More precisely [considering Eqs. (1) and (2), with $M = 1$ and $a = 0$], if we denote the perturbations of the basic state ($\rho = 1$, $u = 0$) by ρ' and u', Tokunaga obtained [9]

$$\rho' = \frac{2\epsilon}{\gamma + 1} [F_1(\xi_1, \tau) - F_2(\xi_2, \tau)], \tag{9}$$

$$u' = \frac{2\epsilon}{\gamma + 1} [F_1(\xi_1, \tau) + F_2(\xi_2, \tau)], \tag{10}$$

where ϵ is the order of magnitude of the nonlinear waves. The new coordinates ξ_i and τ are defined by

$$\xi_i = \epsilon[x - r_i t - \phi_i(x,t)], \tag{11}$$

$$\tau = \epsilon^2 t, \tag{12}$$

where $r_1 = 1$ and $r_2 = -1$ and the phase functions obey

$$\phi_1 = \frac{1}{2}\frac{3-\gamma}{1+\gamma}\int^{\xi_2} F_2(\xi,\tau)d\xi + \theta_1, \tag{13}$$

$$\phi_2 = -\frac{1}{2}\frac{3-\gamma}{1+\gamma}\int^{\xi_1} F_1(\xi,\tau)d\xi + \theta_2, \tag{14}$$

with θ_i arbitrary constants determined by the initial conditions. Finally, the functions F_i (simply related to the Riemann invariants $z^{\pm}$) satisfy the Burgers equations

$$\partial_\tau F_i + F_i \partial_{\xi_i} F_i = \frac{\nu}{2}\partial_{\xi_i\xi_i} F_i. \tag{15}$$

The fields F_i evolve almost independently with the same dynamical equation, except for phase shifts, which are higher order effects that are most important during shock wave collisions. Given initial conditions for ρ' and u', the substitutions $\rho \to 1/\rho$ (or $\rho' \to -\rho'$) and $\gamma \to 2-\gamma$ lead to the replacement of F_1 and F_2 by $F_2(3-\gamma)/(1+\gamma)$ and $F_1(3-\gamma)/(1+\gamma)$, respectively. For a vanishingly small viscosity ν, the rescaling of the amplitudes F_1 and F_2 can be absorbed in a rescaling of the variables ξ_i. Except for this stretching of space and time variables, the dynamics obtained after this substitution leads to the same fluctuations occurring at different locations. As a consequence, we can expect that the probability density functions of the cases γ and $2-\gamma$ for small values of M will be closely related after the change $\rho \to 1/\rho$. The case of higher Mach numbers is more delicate due to the additional problem of mass conservation, rendering a symmetry between ρ and $1/\rho$ impossible. This question is addressed below.

(iii) The substitution $\gamma \to 2-\gamma$ can also be examined at the level of Eqs. (3) and (4). Its effect is simply to change the sign of the right-hand sides. For $\gamma < 1$, Eq. (4) shows that positive values of v (in this case associated with density peaks) are mostly created by shocks (associated with negative velocity gradients). Looking at Eq. (3), we see that as v increases, the pressure term becomes exponentially small and thus cannot prevent the formation of very strong peaks. Negative values of v (associated here with density voids) are created by expansion waves, but in that case the pressure increases exponentially with decreasing values of v leading to a rapid saturation of this process. As a consequence, we expect that for $\gamma < 1$ the PDF of v will be significantly more populated at positive rather than at negative values. For γ larger than unity the PDF of v will be similar, the formation of positive values of v (now associated with density voids) being still unhindered by the pressure. It follows that the PDF of $s = \ln\rho$ for $\gamma > 1$ will appear similar to that for $\gamma < 1$ after we change $s \to -s$.

(iv) When $\gamma = 1$, the behavior is very different since the acceleration due to the pressure term is simply proportional to $-\partial_x s$, and thus never becomes negligible. We expect a symmetry in the PDF of s, positive and negative values of s being equally created, by shocks and expansion waves, respectively.

(v) It is also useful to discuss the shock jump relations for the polytropic equations. Denoting by X the ratio of the post-shock to the pre-shock density, we have (see [2])

$$X^{1+\gamma} - (1+\gamma m^2)X + \gamma m^2 = 0, \tag{16}$$

where m is the upstream Mach number in the reference frame of the shock. This equation shows that for $\gamma = 1$, $X = m^2$, and that the jump X increases more slowly than m^2 for $\gamma > 1$, while it increases faster than m^2 for $\gamma < 1$ with, as $\gamma \to 0$, $X \sim e^{m^2}$. For weak shocks, we get $X \approx 1 + (m^2 - 1)[2/(1+\gamma)]$. In this case, with the shock velocity close to the sound speed, we can write $m = 1 + (u/2c)$, where u is the velocity in the simulation frame, leading to $X = 1 + \Delta\rho/\rho = 1 + (u/c)[2/(1+\gamma)]$. We thus get $\Delta\rho/\rho \sim m_s 2/(1+\gamma)$, with $m_s = u/c$ denoting the Mach number in the simulation frame.

(vi) Additional insights into the level of density fluctuations can be obtained by studying the balance between the various terms in the equations. For almost incompressible turbulence, the balance between the pressure gradient and the nonlinear term in the momentum equation ensures that typical pressure fluctuations scale like $\tilde{M}^2$, where the turbulent Mach number is defined as $\tilde{M} = u_{\rm rms}/c$ (here $u_{\rm rms}$ is mostly made of solenoidal motions, unlike in our 1D simulations where it stands for purely compressible modes). If entropy fluctuations are not allowed (as with a polytropic state law), the resulting density fluctuations also have to scale as $\tilde{M}^2$. In thermally forced turbulence, however, a Boussinesq-like balance occurs between temperature and density fluctuations, maintaining pressure fluctuations of order $\tilde{M}^2$, while allowing for much larger values of density and temperature fluctuations [11].

In weakly nonlinear acoustics, the pressure term is balanced by the velocity time derivative and we recover the scaling $\delta\rho/\rho \sim \tilde{M}$ obtained for weak individual shocks.

B. The case $\gamma = 1$

The main idea of our model is that density fluctuations are built up by a hierarchical process [5]. After a shock (or, respectively, an expansion wave) passes through a given region of mean density ρ_0, the density reaches a new value ρ_1, larger (or, respectively, smaller) than ρ_0. In this region new fluctuations can be created, changing the local value ρ_1 to ρ_2, and so on. Of course the dynamical equations constrain this process. For example, due to mass conservation, arbitrarily high values of the density can only be reached in very localized and thin peaks. We thus expect this hierarchical process to saturate at some value $s_+ > 0$. A similar saturation should occur for low densities at some value $s_- < 0$, with probably $|s_-| > |s_+|$, since larger voids can be created without violating the mass conservation constraint. In the case of the voids, the filling factor is bounded indirectly because, in order to create voids, it is necessary to have peaks, whose filling factor is limited by mass conservation.

The buildup of these density fluctuations is a random multiplicative process which, at the level of the variable s, is additive. Since for $\gamma=1$ the equations are invariant under the change $s\to s+s_0$, the random variable s is the sum of identical random variables, with the individual density jumps all having the same average magnitude, related to the Mach number of the flow, but independent of the local density. The sum of identical random processes is known to have a Gaussian distribution, due to the central limit theorem, no matter what the distribution of the individual processes is. The PDF of s is thus expected to follow a normal distribution.

The variance of the random variable s can be estimated from the strength of the typical shocks and expansion waves. The case of shock waves has been discussed above. At small values of M, $\rho_{i+1}/\rho_i\sim 1+\tilde{M}$, so that $\delta s=\ln(\rho_{i+1}/\rho_i)=\ln(1+\delta\rho/\rho)\approx\ln(1+\tilde{M})\sim\tilde{M}$. At high Mach numbers, individual jumps obey $\Delta s\sim \ln\tilde{M}^2$. For expansion waves, the balance of the time derivative of s and of the positive velocity gradient in Eq. (6) gives $s\sim M$, regardless of the value of M. Indeed, us_x is smaller than s_t because between shocks ρ has a plateau, in which s_x is nearly zero, while s_t is of order unity (note that the decrease of ρ is exponential in time). The density thus decreases in the center of expansion waves while it increases on the edges, until pressure blocks the process. In the case $\gamma=1$, the effect of pressure is symmetric in s so that positive and negative fluctuations are of the same order of magnitude, which itself is much larger than those due to shocks. We thus expect $\sigma_s\sim\tilde{M}$ for a large range of values of the Mach number.

From the previous discussion we can expect the PDF of the variable s to be given by

$$P(s)ds=\frac{1}{\sqrt{2\pi\sigma_s^2}}\exp\left(-\frac{(s-s_o)^2}{2\sigma_s^2}\right)ds, \qquad (17)$$

with $\sigma_s^2=\beta\tilde{M}^2$, and β as a proportionality constant. The maximum of this distribution s_o is simply related to σ_s due to the mass conservation constraint. Writing $\langle\rho\rangle=\int_{-\infty}^{+\infty}e^sP(s)ds=1$ we find $s_o=-\frac{1}{2}\sigma_s^2$ [see Eq. (23) below]. Note that the PDF of ρ is related to that of s by $P_\rho(\rho)=P(\ln\rho)/\rho$.

The predictions of this model can be tested against results of numerical simulations. Figure 1 (top panel) shows a plot of $\log_{10}(\sigma_s)$ vs $\log_{10}(\tilde{M})$ obtained by combining data from several simulations with $M=0.5$, 1, 2, 3, 4.5, 6, and 10. These data were obtained by computing $\tilde{M}$ and σ_s for the accumulated density and velocity fields over groups of 100 consecutive outputs of the simulations (spanning a duration of 10 time units each) for each point in Fig. 1. This plot shows that $\sigma_s^2\approx\beta\tilde{M}^2$, with $\beta\approx1$, with a very good accuracy, up to the highest Mach numbers reached in our simulations. On the other hand, we see in the bottom panel of the same figure, which displays $\log_{10}\sigma_\rho$ vs $\log_{10}\tilde{M}$, that the density standard deviation also scales like $\tilde{M}$ for small values of $\tilde{M}$, while for $\tilde{M}\gtrsim0.5$ the points curve up, a reflection of the relation $\sigma_\rho^2=e^{\sigma_s^2}-1$ between the two variances when ρ obeys a log-normal distribution. The relation $s_o=-\frac{1}{2}\sigma_s^2$ is also well verified numerically as can be seen from Fig. 2.

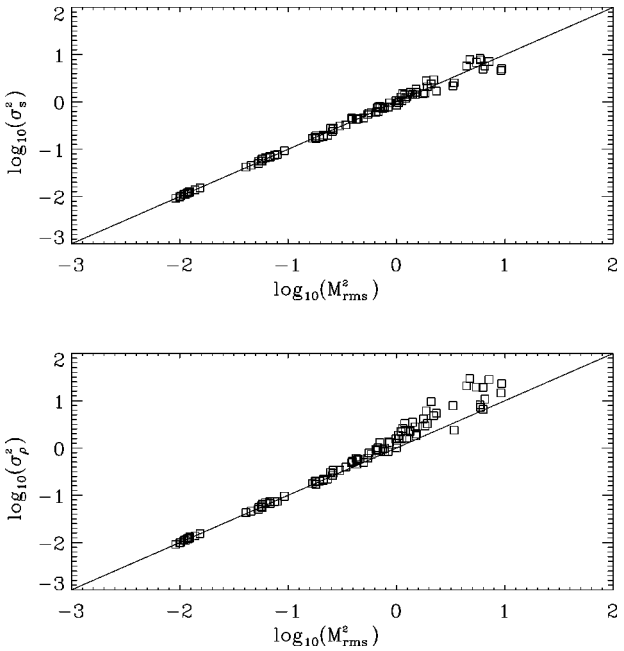

FIG. 1. (Top) Variance of $s=\ln\rho$ vs the mean square Mach number $M_{\rm rms}^2=\tilde{M}^2$ for various simulations with $\gamma=1$ and $M=0.5$, 1, 2, 3, 4.5, and 6. Every point in this plot gives the variance and $\tilde{M}$ over sets of 100 consecutive outputs (10 time units) of any given simulation. The simulations were typically run for 150 time units. (Bottom) Variance of ρ vs $\tilde{M}$.

We now display in Fig. 3 the logarithm of the s histograms for three runs with $\gamma=1$ and $M=0.5$, 2, and 6. Fits with parabolas are shown in dashed lines and show that, to a very good approximation, the density PDFs are log-normals in all three cases. An estimation of the widths and maxima of

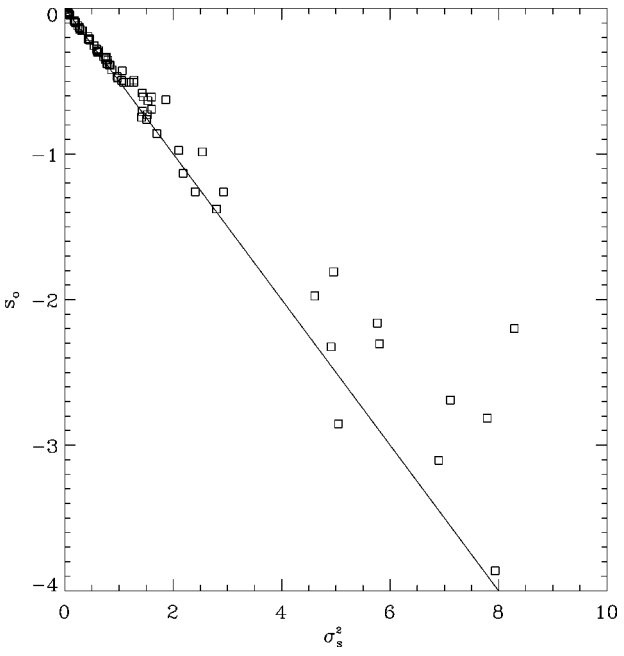

FIG. 2. Most probable value of s vs the variance of s, σ_s^2, for the runs in Fig. 1. The data points are obtained as in Fig. 1.

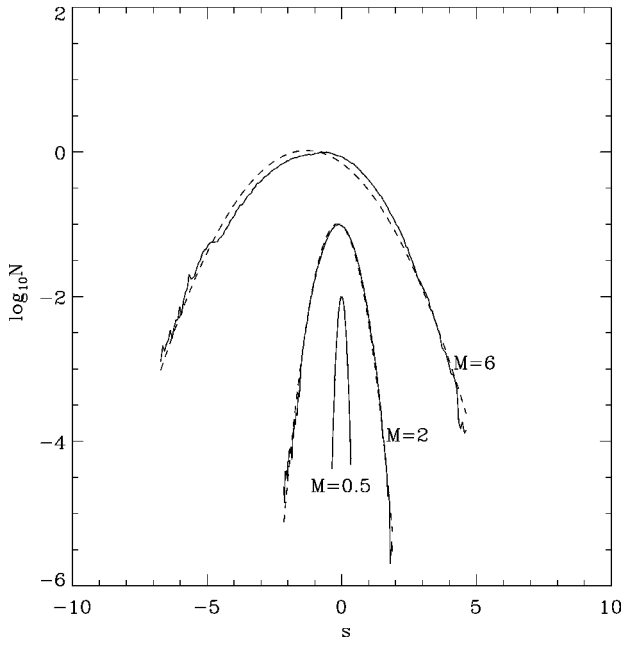

FIG. 3. Probability density function (PDF) of s for three simulations with $\gamma=1$ and $M=0.5$, 2, and 6. For clarity, these PDFs have been respectively displaced in the plot by -2, -1, and 0 units on the vertical axis. The shift of the peak towards more negative s values at larger M is real, due to the constraint of mass conservation. The dashed lines show the best fit with a log-normal to each PDF.

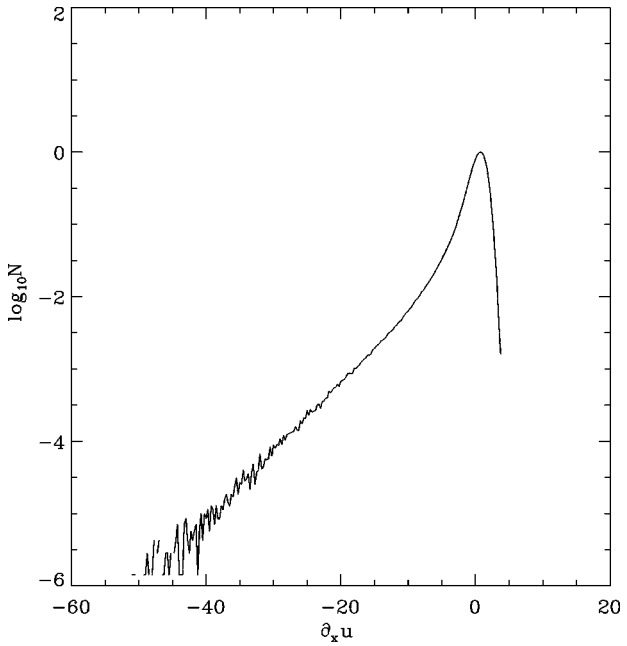

FIG. 4. PDF of the velocity derivative for a run with $\gamma=1$ and $M=6$.

these distributions also shows a very good agreement with the predictions $\sigma_s \approx M$ and $s_o = -0.5\sigma_s^2$.

The distribution of the velocity derivative u_x is shown in Fig. 4 for $\gamma=1$ and $M=6$. This distribution is found to be almost independent of the Mach number. It presents a long exponential tail for negative values of u_x and a strong dropoff for large values, analogous to the one found in the Burgers case [7].

C. The case $\gamma \neq 1$

The difference between the case $\gamma=1$ and the case $\gamma \neq 1$ lies in the behavior of the pressure term as a function of the local density of the fluid, an effect that is most visible after comparing Eq. (3) with Eq. (5). With the density-dependent rescaling $M \rightarrow M(s;\gamma) = Me^{[(1-\gamma)/2]s}$, the two equations are identical, which only means that when $M(s_c;\gamma)$ is substituted for M in Eq. (3), the small fluctuations around $s=s_c$ are identical to those of the case $\gamma=1$.

The argument at the origin of the PDF of s in the isothermal case is based on the fact that the local Mach number of the flow is independent of the local density. When $\gamma \neq 1$ this property is violated and there is no reason to expect a log-normal PDF for the density. We nevertheless propose a heuristic model, reproducing most of the features of the PDFs obtained in our simulations, which consists of taking the functional form of the PDF of the isothermal case and replacing $\tilde{M}$ by $\hat{M}(s;\gamma)$, where $\hat{M}(s;\gamma)$ now stands for the ''effective'' rms Mach number at the value s. This ''effective'' rms Mach number is defined as

$$\hat{M}(s;\gamma) = \begin{cases} \hat{M}(s_+;\gamma) & s > s_+ \\ Mu_{\rm rms}/c(s) = Mu_{\rm rms}\exp[(1-\gamma)s/2] & s_+ \geqslant s \geqslant s_- \\ \hat{M}(s_-;\gamma) & s_- > s. \end{cases} \tag{18}$$

The cutoffs s_+ and s_-, which, as we shall see, are necessary for convergence, are also physically meaningful, since the probability of new fluctuations arising within previous peaks or voids decreases as the amplitudes of the latter become larger because the fraction of space they occupy decreases. The fact that the cutoff occurs at larger values of $|s|$ for $s<0$ than for $s>0$ is due to the larger filling factors of low density regions [see Figs. 5(a) and 5(b) for comparison]. A numerical check of this saturation property is possible if one computes the scatter plot of the standard deviation for s vs the mean value of s in subregions of the integration domain for each snapshot. Figure 6 shows these plots for $M=6$, $\gamma=0.5$, and $\gamma=1.5$ in subregions of length $N/3$. Note that, similar to the $\gamma=1$ case, σ_s is related to $\tilde{M}$, because the two are roughly proportional at low $\tilde{M}$, although they deviate from proportionality at larger rms Mach numbers (see below). Thus, Fig. 6 can also be interpreted as giving the variation of the local Mach number with the local mean density, showing that a clear trend exists. Moreover, we see that the saturation level for $s<0$ at $\gamma=1.5$ occurs at a much higher value of the Mach number than for $s>0$, $\gamma=0.5$. Plots of σ_s and σ_ρ vs $\tilde{M}$ for $\gamma=0.5$ and $\gamma=1.5$ are also presented in Figs. 7 and 8. They show that σ_s increases more slowly than linearly with $\tilde{M}$ for high Mach numbers. This results from the asymmetry in the fluctuations of s for $\gamma \neq 1$. While for $\gamma=1$ the typical excursions of s are of the order of $\tilde{M}$ both

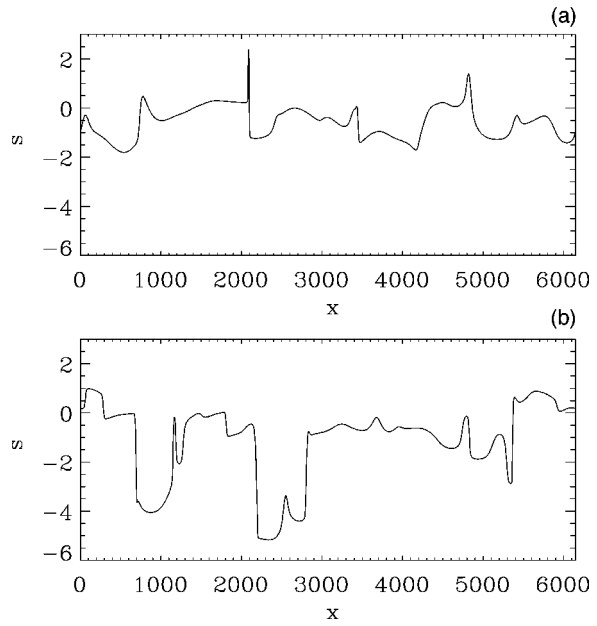

FIG. 5. (a) Density field of a run with $\gamma=0.5$ and $M=10$ at time $t=34.65$. Note the very thin density peaks and the shallow density minima. (b) Density field of a run with $\gamma=1.5$ and $M=6$ at $t=50.5$. Note that the density maxima are now much shorter, while the density minima (voids) become much deeper. They are also much wider than the peaks in the $\gamma=0.5$ case because of mass conservation.

for positive and negative values of s; when $\gamma>1$, for example, pressure blocks the negative fluctuations of s while still allowing for fluctuations of order $\tilde{M}$ on the positive side. The resulting variance σ_s is thus expected to be smaller than

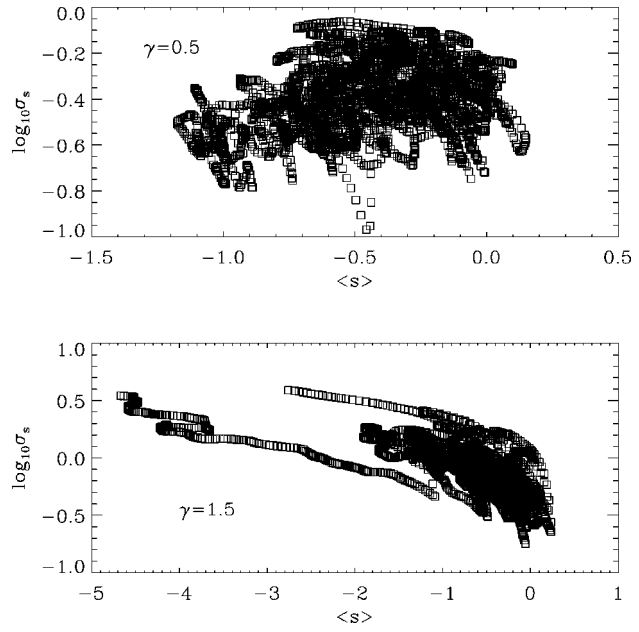

FIG. 6. Standard deviation of s vs the mean value of s over subregions of size 1/3 of the integration domain for two runs with (top) $\gamma=0.5$ and (bottom) $\gamma=1.5$. Note the inverse trends between the two runs and the saturation of σ_s at large values of $|\langle s\rangle|$, especially noticeable in the case $\gamma=1.5$. Note also that σ_s is related to the rms Mach number, as shown in Figs. 7 and 8.

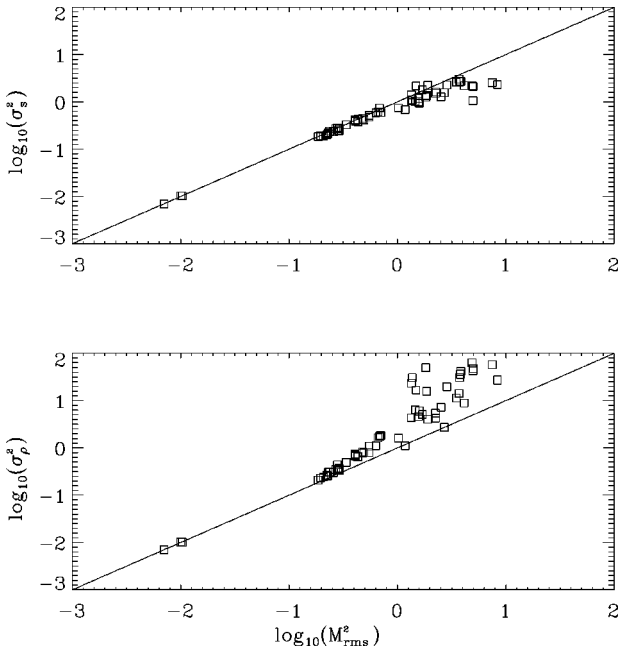

FIG. 7. Variance of s (top) and of ρ (bottom) vs the mean square Mach number for six runs with $\gamma=0.5$ and $M=0.5$, 2, 3, 4.5, 6, and 10. Note that σ_s^2 increases more slowly than $M_{\rm rms}^2$ because only one side ($s>0$) of the density PDF is unimpeded by the pressure. Instead, σ_ρ^2 increases more rapidly than $M_{\rm rms}^2$ because such fluctuations in s imply very large fluctuations in ρ.

$\tilde{M}$. The same argument applies for $\gamma>1$ but then fluctuations are of smaller magnitude when $s>0$. Looking at the plot of σ_ρ we see opposite trends for $\gamma>1$ and $\gamma<1$. First, note that we do not expect the specific relation mentioned above between the variances of s and ρ, since the distribution of s is not Gaussian. Second, this trend is easily interpreted if we recall that for $\gamma<1$ the density fluctuations are in high peaks, while for $\gamma>1$ they consist of large voids. In the former case the variance of ρ can increase greatly when M is large, while in the latter case the voids do not contribute much to the variance, leading to a slower increase of σ_ρ with $\tilde{M}$.

The PDF will thus read

$$P(s;\gamma)ds=C(\gamma)\exp\left[-\frac{s^2}{2\hat{M}^2(s;\gamma)}-\alpha(\gamma)s\right]ds, \quad (19)$$

where $C(\gamma)$ is a normalizing constant such that $\int_{-\infty}^{+\infty}P(s;\gamma)ds=1$. The parameter $\alpha(\gamma)$ is again determined by the constraint of mass conservation stating that the mean value of the density should be 1: $\int_{-\infty}^{+\infty}e^sP(s;\gamma)ds=1$. For $s_-<s<s_+$, Eq. (19) can be written more explicitly as

$$P(s;\gamma)ds=C(\gamma)\exp\left[-\frac{s^2e^{(\gamma-1)s}}{2M^2}-\alpha(\gamma)s\right]ds. \quad (20)$$

Note that in the absence of cutoffs, the convergence of the integrals requires $\alpha>1$ for $\gamma<1$ and $\alpha<0$ for $\gamma>1$. This functional form of the PDF immediately allows us to make a few predictions. For $\gamma<1$, $\hat{M}(s;\gamma)$ grows exponentially with s for $s_-<s<s_+$ and, as a consequence, the PDF for

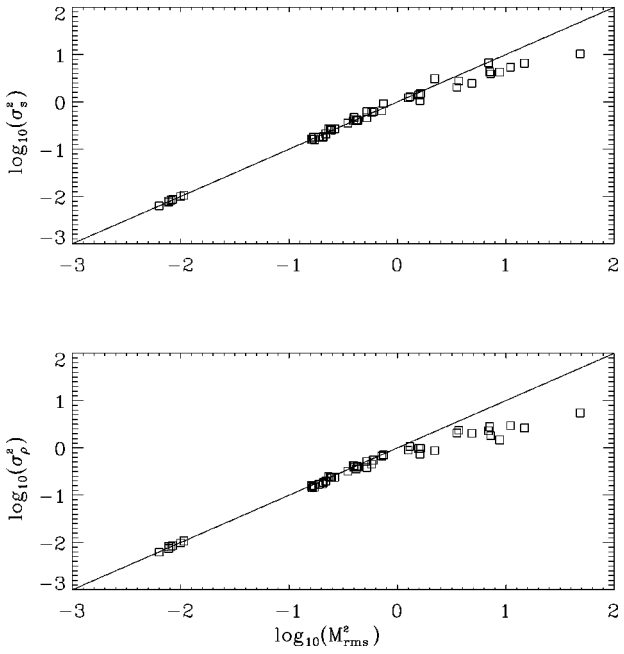

FIG. 8. Variance of s (top) and of ρ (bottom) vs the mean square Mach number for six runs with $\gamma=1.5$ and $M=0.5$, 2, 3, 4.5, and 6. Again (compare to Fig. 7), σ_s^2 increases more slowly than $M_{\rm rms}^2$ because only one side $s<0$ of the PDF is unimpeded by the pressure. However, in this case σ_ρ^2 also increases more slowly than $M_{\rm rms}^2$, because the density fluctuations are bounded by zero, and are not able to contribute much to the variance of ρ.

$0<s<\hat{M}(s;\gamma)$ is dominated by the power-law (in ρ) behavior $P(s;\gamma)\sim e^{-\alpha(\gamma)s}$, while the Gaussian-like decay dominates again for $s>\hat{M}(s;\gamma)$. For $s<0$, the local turbulent Mach number decreases with s and we expect a more rapid dropoff of the PDF than for the case $\gamma=1$ in the same s range. The behavior is exactly opposite when $\gamma>1$. These predictions can be verified by looking at Fig. 9, which displays the PDF of s for $\gamma=0.3$ and $\gamma=1.7$ at $M=3$. The PDF for $\gamma=1.7$ and $M=3$ displays a bump for $s\approx-2$ due to a large, long-lasting void. In order to test whether this feature is due to a rare event, we continued the run for another 150 time units and performed the PDF both for the second part of the run only and for the combined 300 time units. The PDF of the second part presents a nice power law without bump (not shown), while the PDF of the full run presents a milder bump, indicating that very long runs are indeed needed in order to obtain smooth PDF wings.

It is now interesting to relate the PDF for a certain value of γ to that obtained for $2-\gamma$. Writing the condition $\langle\rho\rangle=1$, we get

$$\int_{-\infty}^{\infty}\exp\left(-\frac{s^2}{2\hat{M}^2(s;\gamma)}+[1-\alpha(\gamma)]s\right)ds = \int_{-\infty}^{\infty}\exp\left(-\frac{s^2}{2\hat{M}^2(s;\gamma)}-\alpha(\gamma)s\right)ds, \qquad (21)$$

while the same condition for $2-\gamma$ reads, after making the substitution $s\to-s$ in the integrals,

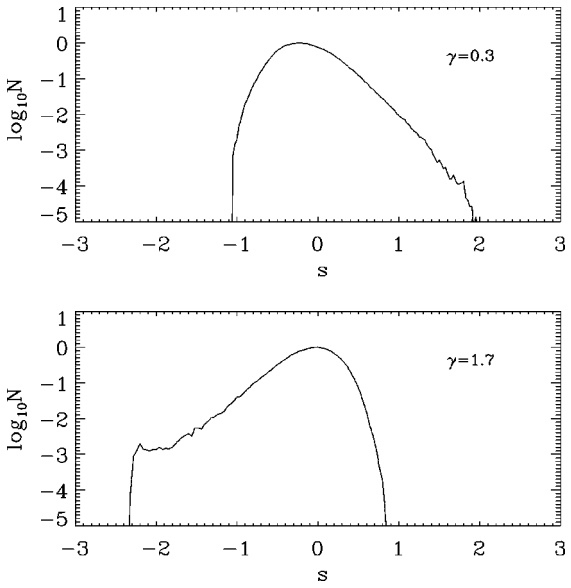

FIG. 9. PDFs of s for two simulations with $M=3$ and $\gamma=0.3$ (top) and $\gamma=1.7$ (bottom). For $\gamma=0.3$ the power-law regime appears at large densities, while for $\gamma=1.7$ it appears at small densities.

$$\int_{-\infty}^{\infty}\exp\left(-\frac{s^2}{2\hat{M}^2(-s;2-\gamma)}-[1-\alpha(2-\gamma)]s\right)ds = \int_{-\infty}^{\infty}\exp\left(-\frac{s^2}{2\hat{M}^2(-s;2-\gamma)}+\alpha(2-\gamma)s\right)ds. \qquad (22)$$

For $s_-<s<s_+$, the functions $\hat{M}(s;\gamma)$ and $\hat{M}(-s;2-\gamma)$ are identical. If the cutoffs s_+ and s_- occur at large enough values, i.e., when the local Mach number is either very large or very small (cf., Fig. 6), the contributions to the integrals of the two terms involving these two quantities will be very close and, by inspection of Eqs. (21) and (22), we get

$$\alpha(2-\gamma)=1-\alpha(\gamma). \qquad (23)$$

This relation is exact when $\gamma=1$ since $\hat{M}(s;1)=\tilde{M}$ is independent of s, allowing us to recover the result $\alpha(1)=\frac{1}{2}$. Note also that for large enough M, a case where Eq. (23) holds, the symmetry $s\to-s$ is not possible but must include a translation in the s domain to account for mass conservation.

Relation (23) is verified numerically with a reasonable precision for the runs at the highest Mach numbers. For example, when $M=6$, the slope of the power law is -1.2 (i.e., $\alpha=1.2$) for $\gamma=0.5$, while we have $\alpha=-0.28$ for $\gamma=1.5$ (see Fig. 10). For smaller values of M, the absolute values of the slopes are closer to each other, a feature due to the different cutoffs for negative and positive values of s (see Fig. 9 for $M=3$ and $\gamma=0.3$ and 0.7). Note that the shape of the PDF for $M=6$, $\gamma=1.5$ exhibits a steeper slope for values of s slightly smaller than that of the maximum. This feature can also be reproduced with this simple model, as can be seen in Fig. 11, which displays the PDF obtained from Eq. (19) for

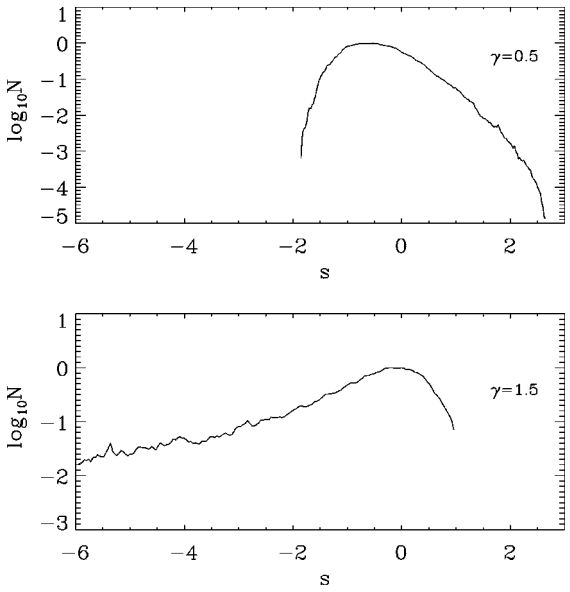

FIG. 10. PDFs of s for two simulations with $M=6$ and $\gamma=0.5$ (top) and $\gamma=1.5$ (bottom). Note that at this Mach number, the power-law regime for the $\gamma=1.5$ case appears removed from the peak of the distribution, mediated by a regime with a steeper slope.

$\alpha=0.28$, $\gamma=1.5$, $\tilde{M}(0)=1.2$, and values of the cutoffs at $\tilde{M}=10$ for $s<0$ and $\tilde{M}=0.1$ for $s>0$.

D. The case $\gamma=0$, i.e., the Burgers equation

An interesting problem concerns the high Mach number limit. It is often suggested that when M is very large, the dynamics of compressible flows should be analogous to that prescribed by the Burgers equation. While this may be true for the velocity field, our results prove that it cannot be the case for the density. Indeed, we find that whatever the value of $\gamma\neq 0$ and of the Mach number, there is always a range of densities for which the pressure cannot be neglected. For that range of densities the PDF has no power-law tail but presents a more rapid dropoff. For $\gamma=1$, it turns out that the pressure is never negligible. Extrapolating our results, we thus predict that for the Burgers case there should be power-law tails both for low and high densities. We have thus performed a simulation of the Burgers equation [coupled with Eq. (2) for the density] with the same parameters as for the previous runs and with $N=6144$. The resulting PDF is presented in Fig. 12. This plot shows that the PDF is indeed almost flat for $s<0$, while there is also a power law for $s>0$, with a negative slope of roughly -0.5. The cutoff for large densities is due to the viscous terms, which give a minimum scale for the width of the shocks, and thus a maximum value for the density peaks. In the physical domain, we observe the creation of voids (s reaching a value of -85 at $t=64$) that occupy most of the domain, together with very high peaks ($s\approx 6.5$). The number of peaks decreases during the simulation while the density in the voids decreases exponentially in time. The forcing is unable to break the peaks because it acts at large scales, while the density fluctuations become as narrow as allowed by viscosity. This PDF has to be contrasted with the one obtained in [7], for which the Reynolds number was low and the simulation was decaying. In that case the power law at high densities was obtained but the PDF presents a sharp dropoff for low densities. Two-dimensional decaying simulations of the Burgers equation are also presented in [8] for moderate Reynolds numbers. The plateau of the PDF at low values of the density is also obtained. Burgers simulations for the decaying infinite Reynolds number case are presented in [12]. In that case the PDF is calculated for the cumulated mass function and not for the density, which is not defined after the first shock formation. A power law is found that extends to $s=-\infty$ and connects to an exponential decay for $s\to+\infty$. Note that an exponential PDF for the density was predicted in [13] on the basis of a model that treats shocks as completely inelastic particles. The case of the forced Burgers equation has also been investigated analytically using the instanton technique ([14] and [15]) and the operator product conjecture [16]. In these works, special attention was devoted to the tails of the velocity difference PDF, for both positive [14] and negative [15] gradients. A numerical investigation aimed at testing these predictions would be of interest but deserves a separate study. It would also be interesting to use the instanton technique to

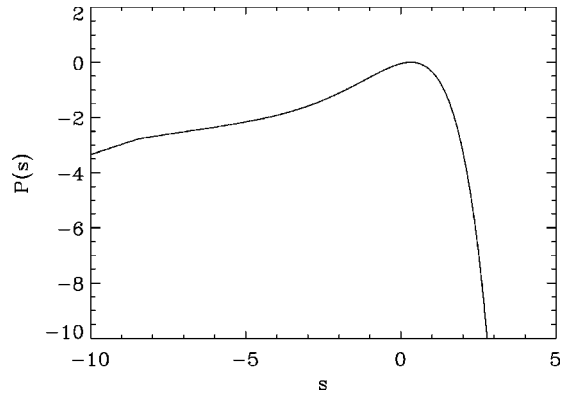

FIG. 11. The theoretical PDF given by Eq. (19) for $\alpha=0.28$, $\gamma=1.5$, $\tilde{M}(0)=1.2$, and values of the cutoffs at $\tilde{M}=10$ for $s<0$ and $\tilde{M}=0.1$ for $s>0$. Compare to Fig. 10.

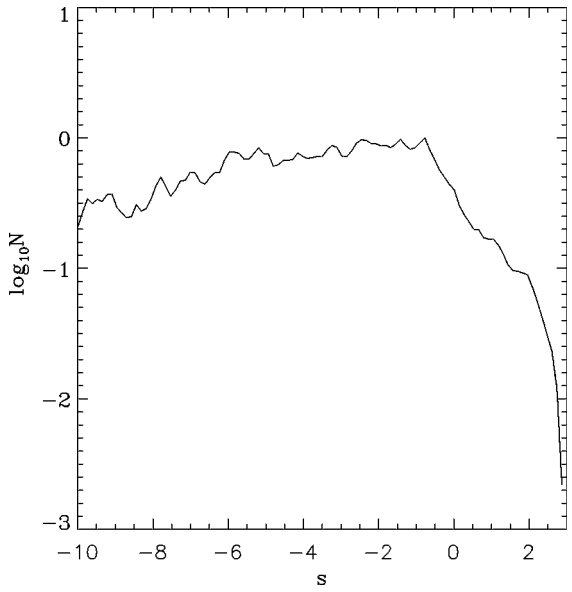

FIG. 12. PDF of s for a Burgers run. Note the nearly flat slope at negative s values.

study the density PDF. To conclude this section, we emphasize that the Burgers case is truly a singular limit that cannot be reached as the high Mach number limit of a polytropic gas, with $\gamma \neq 0$. This is true even for very small values of γ as confirmed by a run with $\gamma = 0.001$ and $M = 10$ from which we obtain a density PDF similar to that of Fig. 10 for $\gamma = 0.5$.

IV. DISCUSSION

A. Effects of the forcing

The study presented in this paper has been performed for a single choice of the forcing and of the Reynolds number. While the variation with the latter parameter can be trivially extrapolated, we cannot *a priori* be sure that our results are independent of the type of forcing. We have performed decay runs and observed that the behavior of σ_s vs $\tilde{M}$ is still the same as in the forced case. The PDFs, however, cannot be computed in a single snapshot due to poor statistics, and cannot be integrated in time since the Mach number changes by roughly 1 or 2 orders of magnitude during the run. We have also performed a run at $\gamma = 1$ with a forcing of the form f/ρ in Eq. (1). In that case the density PDF is not a log-normal anymore but presents a power-law tail for low densities (not shown). This can be attributed to the fact that the flow is stirred more vigorously at low densities so that the effective Mach number indeed increases as ρ decreases. We nevertheless think that our results can be extrapolated to an unforced situation at a given time and possibly also to the multidimensional case. Note that the Mach numbers we have explored in this paper would correspond to even higher Mach numbers in the multidimensional case since then only a fraction of the total kinetic energy populates the compressible modes.

B. Summary

We have presented an investigation of the density PDFs of a randomly accelerated polytropic gas for different values of the polytropic index and of the Mach number. We have suggested a simple model in which the density field is constructed everywhere by a random succession of jumps [5]. When the flow is isothermal ($\gamma = 1$), the jumps are independent of the initial density, and always have the same probability distribution. Expressed in the variable $s \equiv \ln \rho$, the jumps are additive, and by the central limit theorem are expected to have a Gaussian PDF, or a log-normal in ρ.

An analysis of the expected s increments in the weak and strong shock cases, as well as those due to expansion waves, suggested that the variance σ_s^2 should scale as the mean square turbulent Mach number $\tilde{M}^2$. Moreover, because of mass conservation, the peak of the distribution s_o is related to the variance by $s_o = -\frac{1}{2}\sigma_s^2$. These predictions are verified in 1D simulations of compressible turbulence. Previous claims that it is the *density* variance σ_ρ^2 that should scale as $\tilde{M}^2$ [6] might have been misled by lower effective Mach numbers than those achieved in the present simulations, in which all of the kinetic energy is in compressible modes thanks to the one dimensionality.

When $\gamma \neq 1$, the density jumps are not independent of the local density anymore, and the shape of the PDF should change. Observing that a renormalization of the Mach parameter [Eq. (1)] $M \rightarrow M(s;\gamma) = Me^{[(1-\gamma)/2]s}$ restores the form of the equations for the case $\gamma = 1$, we proposed the ansatz that the PDF may still be described by the same functional form as in the case $\gamma = 1$, but replacing M with $M(s;\gamma)$. This prediction is confirmed by the numerical simulations, giving PDFs that are qualitatively in very good agreement with the model PDF, Eq. (19). The result is that the PDF asymptotically approaches a power law on the side where $(\gamma - 1)s < 0$, while it decays faster than log-normally on the other side.

Upon the replacements $\gamma \rightarrow (2-\gamma)$ and $\rho \rightarrow 1/\rho$ we find, using the condition of mass conservation, that the slope α of the power law for a given value of γ is related to its value at $2-\gamma$ by Eq. (23) in the large Mach number limit. These results are also confirmed by the numerical simulations, which exhibit a power law at $s > 0$ when $\gamma < 1$ and at $s < 0$ when $\gamma > 1$, with slopes that are roughly related by Eq. (23), with better accuracy at large Mach numbers.

Finally, on the basis of these results, we suggested that the Burgers case should develop a power-law PDF at both large and small densities, since in this case there is no pressure on either side. This result was again confirmed by a simulation of a Burgers flow.

We conclude this paper by pointing out that the nonuniqueness of the infinite Mach number limit might have important consequences for astrophysical applications, such as in cosmology. The so-called Zeldovich [17] approximation is indeed based on the Burgers equation, which, in light of the present work, appears as a questionable model of highly compressible flows. This point will be addressed in future work.

ACKNOWLEDGMENTS

We gratefully acknowledge financial support from UNAM/CRAY under Grant No. SC-008397, UNAM/DGAPA under Grant No. IN105295 (E.V.-S.), and a joint CONACYT CNRS grant. This work also benefited from partial support from the Programme National du CNRS ''Physique Chimie du Milieu Interstellaire.''

[1] L.D. Landau and E.M. Lifshitz, *Fluid Mechanics* (Pergamon, New-York, 1987).

[2] E. Vázquez-Semadeni, T. Passot, and A. Pouquet, Astrophys. J. **473**, 881 (1996).

[3] Note that γ is simply a parameter here, and that it need not be related to the heat capacity ratio of the gas.

[4] S.A. Balbus, in *The Physics of the Interstellar Medium and Intergalactic Medium*, Vol. 80 of Astronomical Society of the Pacific Conference Series, edited by A. Ferrara, C.F. McKee, C. Heiles, and P.R. Shapiro (ASP, San Francisco, 1995), p. 328.

[5] E. Vázquez-Semadeni, Astrophys. J. **423**, 681 (1994).

[6] P. Padoan, A. Nordlund, and B.J.T. Jones, Mon. Not. R. Astron. Soc. **288**, 145 (1997).
[7] T. Gotoh and R.H. Kraichnan, Phys. Fluids A **5**, 445 (1993).
[8] J. Scalo, E. Vázquez-Semadeni, D. Chappel, and T. Passot, Astrophys. J. (to be published).
[9] H. Tokunaga, J. Phys. Soc. Jpn. **41**, 328 (1976).
[10] T. Tatsumi and H. Tokunaga, J. Fluid Mech. **65**, 581 (1974).
[11] B. Bayly, D. Levermore, and T. Passot, Phys. Fluids A **4**, 945 (1992).
[12] M. Vergassola, B. Dubrulle, U. Frisch, and A. Noullez, Astron. Astrophys. **289**, 325 (1994).
[13] T. Tatsumi and S. Kida, J. Fluid Mech. **55**, 659 (1972).
[14] V. Gurarie and A. Migdal, Phys. Rev. E **54**, 4908 (1996).
[15] E. Balkovsky, G. Falkovich, I. Kolokolov, and V. Lebedev, Phys. Rev. Lett. **78**, 1452 (1997).
[16] A. Polyakov, Phys. Rev. E **52**, 6183 (1995).
[17] Y. Zeldovich, Astron. Astrophys. **5**, 84 (1970).